Photoelectron flux variations observed from the FAST satellite

W.K Peterson[a], T.N. Woods[a], P.C. Chamberlin[a], and P.G. Richards[b]

[a]*Laboratory for Atmospheric and Space Physics, University of Colorado, Boulder, CO 80303, United States*
[b]*Computer Science Department, University of Alabama in Huntsville, 301 Sparkman Drive, Huntsville, AL 35899, United States*

Revised February 2007.

Abstract

This paper examines high resolution ($\Delta E/E = 0.15$) photoelectron energy spectra from 10 eV to 1 keV, created by solar irradiances between 1.2 and 120 nm. The observations were made from the FAST satellite at ~ 3,000 km, equatorward of the auroral oval for the July-August, 2002 solar rotation. These data are compared with the solar irradiance observed by the Solar EUV Experiment (SEE) on the Thermosphere Ionosphere Mesosphere Energetics and Dynamics (TIMED) satellite and fluxes calculated Field Line Interhemispheric Plasma (FLIP) code. The 41 eV photoelectron flux, which corresponds to solar EUV fluxes near 20 nm, shows a clear solar rotation variation in very good agreement with the EUV flux measurements. This offers the possibility that the 41 eV photoelectron flux could be used as a check on measured solar EUV fluxes near 20 nm. Because of unexpected noise, the solar rotation signal is not evident in the integral photoelectron flux between 156 and 1000 eV corresponding to EUV wavelengths between 0.1 and 7 nm measured by the SEE instrument. Examination of daily averaged photoelectron fluxes at energies between 25 eV and 500 eV show significant changes in the photoelectron spectra in response X and M class flares. The intensity of photoelectrons produced in this energy region is primarily due to two very narrow EUV wavelength regions at 2.3 and 3 nm driving Auger photoionization in O at 500 eV and N_2 at ~360 eV. Comparison of calculated and daily averaged electron fluxes shows that the HEUVAC model solar spectrum used in the FLIP code does not reproduce the observed variations in photoelectron intensity. In principle, the 21 discrete photoelectron energy channels could be used to improve the reliability of the solar EUV fluxes at 2.3 and 3 nm inferred from broad band observations. In practice, orbital biases in the way the data were accumulated and/or noise signals arising from natural and anthropogenic longitudinally restricted sources of ionization complicate the application of this technique.

1. Introduction

Solar illumination is the primary energy source driving Earth's thermospheric chemistry and dynamics. Knowledge of the spectral and temporal variations of solar energy input is fundamental to understanding the thermosphere. Early rocket measurements during the 1960s and early 1970s culminated in the production of the F74113 solar reference spectrum that was used extensively along with Atmosphere Explorer-C satellite data to develop the chemical scheme that was highly successful in explaining the aeronomy of the ionosphere and thermosphere. The F74113 reference spectrum covered the wavelength range from 1.4 to 200 nm. A new solar minimum reference spectrum called SC#21REFW was developed following an extensive set of measurements on the Atmosphere Explorer-E satellite from solar minimum in mid 1977 until solar maximum in 1980 and a 1979 rocket measurement [*Hinteregger et al*., 1981]. *Richards and Torr* [1984] uncovered an apparent problem with the solar reference irradiances below 25 nm that showed up as a discrepancy in the shape of theoretical and measured photoelectron flux spectra. The problem could be resolved by increasing the solar EUV flux below 25 nm by a factor of 2. Subsequent measurements from the SNOE and TIMED satellites support this conclusion. There remain ambiguities about the spectral distribution, magnitude and variations of the solar irradiances in the range below 120 nm. Though not as important as magnetic storms, solar radiation in this range is an important driver of ionospheric space weather [Woods and Rottman, 2002]. Our imprecise understanding limits our ability to model and therefore understand thermospheric chemistry.

Dynamic global models of the Earth's thermosphere require observations or reliable estimates of the temporal and spectral distribution of the solar irradiance. In the spectral region below 120 nm, contemporaneous observational needs are partially met by instruments on SOHO [Judge, 1998], SNOE [Bailey et al., 1996], and TIMED/SEE [Woods et al., 1998, 2005] since 1998. However, the SNOE and TIMED/SEE measurements are not continuous in time and are made over broad spectral bands. SOHO and SNOE observations do not cover the full spectral range of interest. Therefore, models have been developed to estimate the solar spectral variability based on many factors including the broadband satellite data from SOHO, SNOE, and TIMED below 27 nm and the observed X-ray flux on the NOAA/GOES satellites (See, for example, Warren et al., 2001, Solomon and Quan, 2005, Chamberlin, 2005, and Richards et al., 2006).

In some spectral ranges, limited information about spectral variability of solar irradiances can be inferred from aeronomic observations. Richards and Torr [1984, 1985] and Goembel et al. [1997] demonstrated that AE in-situ observations of the O/N_2 number densities and simultaneously observed ionospheric photoelectron energy spectra were consistent. Hernandez et al. [1983] compared the AE-C and AE-E photoelectron spectra with measured and calculated N_2 2PG volume emission rates and established that the magnitude of the differences are on the order of 30%. Strickland et al. [2004] developed a technique to use TIMED/GUVI observations and the NRLEUV model to estimate the relative solar irradiance short ward of 45 nm. Woods et al. [2003] demonstrated that data from the FAST Electron ElectroStatic Analyzer (EESA) array [Carlson et al., 2001], from altitudes above the ionosphere reporting the intensity and spectral distribution of the photoelectrons, provide strong constraints on the partitioning of EUV energy measured

with stable but broad-band detectors into more geophysically relevant (i.e. narrower) wavelength bins. As noted in the Woods et al. paper, most investigators now agree that the Atmosphere Explorer reference model EUV fluxes are too low in the region below 27 nm. However, it is not yet clear how the energy in this spectral region should be apportioned from highly stable, broadband, observations made by instruments such as TIMED/SEE into the narrower wavelength bands needed in thermospheric chemistry models.

Richards et al. [2006] reported that the energy dependence of photoelectron spectrum agrees well with that reported from DE-2 by Winningham et al. [1989], and previous observations from the AE satellites by Doering and his colleagues [e.g. Lee et al., 1980]. Given that the energy dependence of the photoelectron spectra depends on relatively stable ionospheric composition and solar irradiance distributions (but not magnitudes) and that the energy dependence of the photoelectron spectrum has been independently confirmed from three different instruments over a period of 30 years, the shape of the photoelectron energy spectrum can be used to partition EUV energy measured in broad bands by the highly stable detectors on TIMED/SEE, SORCE, and SNOE [e.g. Woods and Rottman, 2002, Bailey et al. 1996].

The purpose of this paper is to determine if systematic examination of photoelectron observations, similar to those reported by Woods et al. [2003] can be used, in conjunction with a modeling effort, to address the temporal variability of the photoelectron flux with the variability of the solar irradiance at higher resolution in the 1-7 nm range over a solar rotation.

2. Observations

The photoelectron data were obtained during the solar rotation from July 10 to August 10, 2002. During this solar rotation the daily $F_{10.7}$ index varied from 122 to 242 reaching maximum intensity between July 26 and 28. Also during this period, the SOHO Solar EUV Monitor (SEM) [Judge et al. 1998] measured the solar EUV flux in the 26-34 nm and in the 0.1 to 50 nm ranges. In both channels, the solar EUV flux followed the daily $F_{10.7}$ index but with a maximum increase of ~25% rather than the factor of 2 variation of the daily $F_{10.7}$ index.

Figure 1 presents data acquired by the FAST electron spectrometer [Carlson et al., 2001] on July 20, 2002 during an apogee pass over the northern polar cap. The top panel shows an energy-time spectrogram of the observed upflowing electron energy flux averaged over a 60 degree angular range centered on the magnetic field direction. Energy coverage is from 6 eV to 30 keV. The bottom panel shows an angle-time spectrogram of the angular distribution of the energy spectrum averaged over the energy range from 20 eV to 30 keV. Electron precipitation associated with the auroral zones and polar cap were observed from ~17:00 to ~17:30 UT. The energy-time spectrogram in the top panel shows the well-known feature between 20 and 30 eV associated with photoionization caused by the solar He 30.4 nm emission (e.g. Doering et al. 1976). The solar zenith angle (SZA) at the foot of the magnetic field line passing through FAST ranges from 92^o at 16:48 to 60^o at 17:38.

The intensity of the feature between 20 and 30 eV as well as the entire photoelectron spectra is nearly constant during this interval reflecting the insensitivity of the escaping

photoelectron flux to variations in the SZA when the ionosphere is sunlit (see, for example, Su et al., 1998). There is little dependence on solar zenith angle because photoelectrons that escape the ionosphere are produced above approximately 350 km where, for solar zenith angles below 90^o, attenuation of the solar EUV radiation is small.

The bottom panel of Figure 1 shows three prominent features in the angle-time spectra before ~17:00 and after ~17:30. Photoelectrons emitted from the FAST spacecraft are seen as two narrow emission features centered at 90^o and 270^o. Both of these electron populations have pitch angles near 90^o. The broad feature centered on 180^o in the bottom panel of Figure 1 is the flux of upflowing ionospheric electrons, most of which are the direct result of photoionization processes in the topside ionosphere. Photoelectrons are created with an isotropic angular distribution in the ionosphere but become increasingly field-aligned as the magnetic field intensity decreases with increasing altitude. Conservation of the first adiabatic invariant focuses these ionospheric photoelectrons into the relatively narrow "source cone" centered on the magnetic field direction (180^o) at the 3,000 to 4,000 km observation altitude. Not easily seen in the angle-time spectrogram before 17:00 and after 17:30 are the weak fluxes of downward directed electrons centered on 360^o from the magnetically conjugate hemisphere.

Our objective is to determine to what extent the flux of electrons in the source cone can be used as a proxy for the intensity of the solar irradiance. Electrons that stream up magnetic field lines and are detected by FAST at ~ 3000 km are created by various processes. These processes include photoionization in the local ionosphere, backscatter of photoelectrons from the conjugate hemisphere, and possibly backscatter from other energetic electrons and ions impinging on the ionosphere. The intensity of upflowing photoelectrons is almost independent of neutral composition of the thermosphere because the production and loss of photoelectrons have similar dependencies on the neutral species densities [Richards and Torr, 1983]. The photoelectron flux depends primarily on the intensity of the solar EUV irradiance in the local hemisphere. There is an approximate 30% contribution from photoelectrons that escape from the sunlit magnetically conjugate ionosphere and are mirrored and/or backscattered from the local atmosphere up to the FAST satellite altitude. For energies below approximately 50 eV the escape flux can be attenuated by Coulomb collisions with ambient thermal electrons below 1000 km.

Figure 1 shows that the relative variation of electron fluxes detected by FAST is largest in the auroral zones and polar cap. Since solar illumination, except during solar flares, varies slowly in time, we restrict our investigation to observations made equatorward of the auroral ovals, i.e. on magnetic field lines with foot points in both hemispheres and where auroral electron acceleration processes are not active.

Figure 2 presents an overview of one-minute average electron spectra obtained equatorward of the auroral zones at altitudes well above the ionosphere from July 10 to August 10, 2002. As described in Woods et al. [2003] a small background signal caused by energetic ions and electrons normally found in this latitudinal range has been subtracted. During this interval there were well-documented variations in the intensities of solar EUV and XUV irradiances (e.g. Strickland et al., 2004). The top panel shows an energy-time spectrogram of upcoming electrons with pitch angles between 160^o and 200^o from the 3417 one-minute intervals available for analysis. Because of operational constraints, data were not acquired on every orbit and then only acquired for limited

(typically 10^o) intervals equatorward of the auroral zone. The middle panel in Figure 2 shows the solar zenith angle (SZA) at the ionospheric foot of the magnetic field line descending through FAST.

Intervals where the foot of the field line is not illuminated are characterized by significantly weaker fluxes of upflowing electrons. Because the escaping photoelectrons are produced high in the thermosphere where the atmosphere is thin, significant photoelectron production occurs for solar zenith angle up to ~100 degrees. When the conjugate hemisphere is illuminated, there can be significant photoelectrons fluxes backscattered into the FAST field of view even when the local ionosphere is dark (for example, Peterson et al., 1977). The bottom panel in Figure 2 presents the 2416 average energy spectra obtained where the SZA at the foot of the field line was less than 90^o. Note that the data in Figure 2 are not continuous in time. The widths of the photoelectron spectra presented in Figure 2 are therefore not uniform.

The ionization potentials of major ionospheric constituents lie between 14 and 21 eV. Therefore, the 0.1 nm to 7 nm band (corresponding to energies from ~12 keV to ~177 eV) of Solar XUV energy sampled by the TIMED/SEE instrument generally corresponds to primary photoelectrons with energies from ~156 eV to ~12 keV. Two strong peaks in the photoelectron production rate resulting from the Auger photoionization process dominate the production of photoelectrons in this energy range. The O photoionization cross section has a narrow peak near 2.3 nm (corresponding to photoelectrons of ~500 eV) with a half-width of less than 0.1 nm and the N_2 cross section has a broader peak near 3 nm (corresponding to photoelectrons of ~380 eV) with a half-width of less than 0.5 nm (see Figure 2 of *Richards et al*., 2006). We note that 300-500 eV electrons are responsible for ion production in the E region of the ionosphere near 105 km altitude.

Auger photoelectrons are the dominant source of primary photoelectrons with energies above 300 eV and can therefore be regarded as sensitive monitors of the solar EUV fluxes in very narrow ranges centered at 2.3 nm and 3 nm. The Auger electrons also dominate the photoelectron population between 100 and 300 eV because of the cascade process in which the primary photoelectrons are degraded by collisions with the neutral gases. Thus the 100-600 eV photoelectron flux is useful primarily to monitor the specific solar fluxes at 2.3 and 3 nm. Photoelectron fluxes can be used as a check on 10-30.4 nm solar EUV fluxes that produce photoelectrons between 20 and 100 eV because primary production generally exceeds cascade production through most of this energy range [*Richards and Torr*, 1984, *Richards et al*., 2006].

Beyond 500 eV, the measured photoelectron flux drops rapidly by an order of magnitude and statistically significant fluxes of upflowing photoelectrons greater than ~ 1 keV are observed only during the most intense Solar flare events. We therefore restrict direct comparison of TIMED/SEE data from the 0.1 to 7 nm band to 156 eV to 1 keV electrons (A 1 keV electron is produced by a 1.18 nm photon). Figure 3 presents integral electron fluxes from 156 eV to 1 keV derived from 2416 electron spectra displayed in the bottom panel of Figure 2 and solar irradiances in the 0.1 to 7 nm band measured by the TIMED/SEE instrument [Woods et al., 1998, 2005]. The SEE data in Figure 3 were obtained from the Version 8 distribution. The average FAST electron fluxes have been normalized to the average TIMED/SEE power observed in the 0.1 to 7 nm channel. TIMED/SEE data shown are averages from a ~3 minute interval during each TIMED

orbit. No data were acquired in the 0.1 to 7 nm band from midday on July 24 until July 31 (days 13 to 20 in Figure 3). The TIMED/SEE data show several intense bursts of power associated with solar flares. Because of the intermittent nature of TIMED/SEE data acquisition only a fraction of the solar flares occurring between July 11 and August 13, 2002, are seen in Figure 3. The times of FAST and TIMED observations do not generally overlap. The most obvious conclusion that can be drawn from Figure 3 is that the solar power in the 0.1 to 7 nm band inferred from FAST electron fluxes has considerably more short-term variability than that measured by the TIMED/SEE instrument.

To determine if the larger short-term variability of the electron data is the result of limitations of the electron spectrometer sensitivity we have examined electron spectra from an energy range where detector sensitivity is not an issue. Peterson et al. [1977] have shown that the intensity of photoelectrons bouncing between conjugate ionospheres is most intense below ~ 60 eV. Noise can be introduced into the FAST measurement if the photoelectron spectrum has sharp features because minor variations in the spacecraft potential could significantly change the detector response. Doering et al. [1976] have shown that the solar He II line at 30.4 nm produces intense features in the 20 to 30 eV photoelectron spectra that have energy widths considerably narrower than can be resolved by the FAST electron spectrometer. This may not be a problem at FAST altitudes because the features are smoothed out by Coulomb collisions with ambient thermal electrons. Lee et al. [1980a,b] have shown that the features become washed out at high altitudes as a result of increasing collisions with thermal electrons. There could be variations, perhaps as large as 30%, in the 20-30 eV fluxes at the FAST altitude as a result of different thermal electron densities below 1000 km altitude.

Figure 4 shows data from the FAST electron channel centered on 41 eV which are produced by photons in the wavelength range from ~19 to ~24 nm. In this region, the photoelectron fluxes are significantly above the instrument threshold. The 41 eV flux shows ~20% scatter superimposed on a longer-term modulation with a 25% increase in overall flux until the middle of the period and then a decline. The longer-term variation is consistent with variation in solar activity and is also consistent with the variation in solar 26-34 nm EUV flux measured by the SEM instrument (SOHO Solar EUV Monitor, Judge et al. 1998) during this solar rotation period. The longer-term variation at 41 eV in Figure 4 is larger than that for the integral flux between 156 eV and 1 keV shown in Figure 3. The 20% of the scatter in the 41 eV electron fluxes (10 to 24 nm solar emissions) in Figure 4 is comparable to that for 156 eV to 1 keV electron fluxes (1 to 7 nm solar emissions) shown in Figure 3. We conclude that the scatter in the 156 eV to 1 keV range is not the result of limitations associated with the detector sensitivity. There also appears to be a strong temporal signal in Figure 4 with a period on the order of a day not found in the solar observations. Therefore, there must be sources other than variations in the solar XUV intensity to account for the scatter in the electron flux shown in Figures 3 and 4.

Further investigation reveals that the large short-term variations of the flux intensity in Figure 4 have significant patterns in the spatial domain. Figure 5 presents the 2416 data points in Figure 4 organized by longitude of the ionospheric foot of the field line passing through the FAST satellite. The longitudinal peaks in upflowing electron

intensity in Figure 5 appear to reflect longitudinally restricted sources of ionization that add to the photoelectron source. These longitudinally organized peaks are clearly not associated with variations in the solar XUV intensity. FAST samples an extended longitudinal range of magnetic foot points in each data accumulation interval. For example during the interval shown in Figure 1, data from before ~17:00 were obtained at longitudes from 52^o to 58^o; after ~17:30 longitudes of 208^o to 211^o were sampled. Between 17:00 and 17:30, when FAST was on magnetic field lines in the auroral oval or polar cap and which are not included in Figure 5, the longitude of the foot of the magnetic field line passing through FAST ranged from 58^o to 208^o. Nearer the 90^o and 270^o longitude regions, where the magnetic declination is greater, the longitude sampled in individual FAST orbits and reported in Figure 5 ranges up to 10^o.

The longitudinally restricted maxima shown in Figure 5 could be an artifact of the way the data were acquired and averaged. Most of the data presented above were acquired near FAST apogee (~4,000 km) and near the terminator (i.e. SZA near 90^o). Figure 6 displays the distribution in solar zenith angle (SZA) and altitude of the 2416 average energy spectra shown in the bottom panel of Figure 2.) Figure 7 shows the sampling distribution in altitude as a function of the longitude of the magnetic foot point. The regularly spaced 'dips' in Figure 7 are somewhat related to the locations of minima in the 41 eV upflowing fluxes shown in Figure 5. The relation between the longitudinal dips in Figure 7 and the maxima in Figure 5, however, is not exact and the offsets as a function of longitude are not constant.

The data presented above show that the solar power in the 0.1 to 7 nm band inferred from FAST electron fluxes has considerably more variability than that directly measured by the TIMED/SEE instrument. Figure 5 suggests that some of this variability is related to additional longitudinally restricted sources of electrons. Figure 6 and 7 suggest that some, if not all, of the longitudinal variation could be an artifact of the way the data were acquired and averaged. We address the possible sources of these longitudinal maxima in upflowing electron intensity in the Discussion section below. We also present an alternative way to average and present the data that emphasies the photoelectron response to X and M class solar flares.

3. Discussion

The long-term variation in the 41 eV photoelectron flux over the solar rotation is consistent with the SEM measurements and also with results of Strickland et al. [2004] who investigated and modeled the variation of the solar intensity in the 1-45 nm wavelength region for the same solar rotation period. Specifically, they examined volume emission ratios of O 135.6 nm emissions to N_2 LBH emissions (140 to 150 nm) and combined them with the NRLEUV model [Warren et al., 2001] to derive a measure of the total solar irradiance short ward of 45 nm (corresponding to photoelectrons with energies greater than ~12 eV). They reported variations of this measure, the Q_{EUV} index, of ~20% over the solar rotation. They noted that the unadjusted NRLEUV model predicted slightly larger (~30%) variations of the energy short ward of 45 nm. In data from single orbits, they reported variations in the ratio of O 135.6 nm emissions to N_2 LBH emissions (140 to 150 nm) from 10 to 20%. Strickland et al. attribute the 10 to 20% variation in daily

Q_{EUV} index values to uncertainties in the model and observations. They also report significant (i.e. larger than 20%) impulsive variations in the Q_{EUV} index. They show that these impulsive variations are directly associated with intensifications of emissions in the SEM central channel which is sensitive to the 0.1 to 50 nm range. As noted by Strickland et al, the impulsive variations in Q_{EUV} are most probably related to solar flare events.

The 41 eV photoelectron data shown in Figure 5 and acquired at the same geographic longitude show variation from less than 10% to more than 20%. This variation comes from both real variation in solar irradiance and a noise signal that is organized spatially, i.e. in longitude. There are several known sources for longitudinally restricted regions of ionization in the sub-auroral latitudes considered here. These include broad regions of energetic electron precipitation (~10^o) from natural sources (lighting induced electron precipitation and the South Atlantic Anomaly) and narrow regions of energetic electron precipitation (~1^o) from anthropogenic ELF radio transmitters. It is also possible that an orbital bias in the way the data were acquitted and averaged could account for the longitudinal organization of the data.

Because the measurements are heavily weighted towards the terminator, one possible explanation for the ~30% variation in the observed flux is related to the conjugate solar zenith angle. When both hemispheres are fully illuminated, the backscattering of the conjugate photoelectron flux into the FAST field of view will increase the observed flux by about 30%. Thus an apparent 30% fluctuation could be attained from changes in the conjugate solar zenith angle from fully illuminated to dark. This explanation has the virtue that the variation would be relatively independent of photoelectron energy as is observed. To investigate this possibility, we rebinned the data with local solar zenith angle < 90 degrees and the conjugate solar zenith angle > 103 degrees. This reanalysis did not remove the variability in the observed flux. We therefore conclude that the observed scatter is not a conjugate solar zenith angle effect.

Natural and anthropogenic wave induced electron precipitation caused by whistler waves leads to precipitation of energetic (10 to 100 keV) electrons from the ring current and radiation belt regions of the magnetosphere (see, for example, Datlowe et al., 1995, Rodger and Cliverd, 2002, Sauvaud et al., 2006, and references therein). Energetic electrons are also preferentially precipitated from the ring current in the South Atlantic Anomaly region. (See, for example, Abel and Thorne, 1999). Precipitating energetic electrons from all sources produce ionization at all ionospheric altitudes. Most of the ionization from energetic precipitating electrons occurs below 100 km. (See, for example, Rodger et al. 2002.)

However, energetic electron precipitation is unlikely to be the source of the observed variation in the FAST photoelectron fluxes for three reasons, 1) the backscattered precipitating electron flux spectrum would have a different spectral shape from photoelectrons because it is purely driven by cascade at these low energies. Thus, backscatter from precipitating fluxes would be unlikely to affect the fluxes by ~20% at all FAST energies, 2) such a backscatter flux should be clearly apparent above 600 eV but it is not, and 3) there is no evidence for a precipitating flux when both ends of the flux tube are in darkness, even though waves penetrate into the plasmasphere more easily at night. In addition, there is insufficient information to determine if the regularly spaced 'dips' in

upflowing 41 eV electron flux seen in Figure 7 are directly related to the locations of minima in the 41 eV upflowing fluxes shown in Figure 5.

Figures 6 and 7 suggest that some, if not all, of the noise signal (i.e. the longitudinally organized regions of extra ionization shown in Figure 5) are the result of an orbital bias in the data. To examine this possibility we examined sub sets of the data restricted to intervals with the solar zenith angle less than 80^o or altitude greater than 3,500 km. In both of these data sub sets the longitudinal structured regions of enhanced ionization remained. Further sub setting of the data was not practical because of the limited number of sample intervals and their distribution in time and space. There is also insufficient information to characterize the magnitude and temporal variability of the longitudinally structured noise sources identified here.

Figure 8 displays another way to examine variations of the photoelectron spectrum. Presented in Figure 8 are daily averages of the photoelectron flux at specific energies obtained from FAST and calculated using the Field Line Interhemispheric Plasma (FLIP) code (Richards, 2002) using the HEUVAC solar flux model (Richards et al., 2006). Fluxes at energies between 98 and 486 eV (e-i) show a clear increase on day 5 (July 15) corresponding to an X magnitude solar flare detected by the GOES satellites at 20:08 UT, a time when FAST was observing photoelectrons and the SEE/XPS sensor was not operating. Similar features in the observed spectra on days 10 and 16 (July 20 and 26) correspond to X and M class flares respectively. No FAST data are available during the time of the most intense 0.1 – 7 nm emissions detected by the SEE/XMS sensor on July 23 (day 13). Examination of the variation of photoelectron intensity during solar flares is beyond the scope of this paper. We note, however, that Strickland et al. [2004] have identified and discussed several solar flare events seen in the TIMED/GUVI data from July-August, 2002 interval discussed here.

Figure 8 also shows a peak in the 486 eV (i) flux intensity between days 13 and 25 roughly agreeing with a peak in the calculated fluxes. The HEUVAC solar model is driven primarily by the magnitude of the observed $F_{10.7}$ solar radio flux. The magnitude of the observed peak in the daily average flux decreases with energy and is not detectable below 196 eV (f). However the peak can be seen in all of the calculated energy channels. We conclude that the default distribution of EUV power as a function of wavelength and $F_{10.7}$ in the HEUVAC does not completely capture the variations in wavelength distribution of the solar flux below ~120 nm. Because the magnitude of the unexplained noise in the photoelectron spectra is comparable to the magnitude of the peak in the daily averaged 486 eV fluxes, a more detailed comparison of the calculated and observed data is not justified.

4. Conclusions

We have shown that upflowing photoelectron energy spectra observed near 41 eV, corresponding to solar irradiances between ~19 and ~24 nm vary ~20% between July 10 and August 10, 2002. This variation is consistent with the results reported by Strickland et al. [2004] for the wavelength region short ward of 45 nm. We have also shown that the

magnitude of variation of daily average fluxes increases with energy up to the ~500 eV maximum presented in Figure 8.

Solar power in the 0.1 to 7 nm band inferred from FAST electron fluxes in the 156 eV to 1 keV has considerably more variability than that directly measured by the TIMED/SEE instrument. We found that most of the electron flux in this energy range comes either directly or in cascade processes from Auger photoionization near 500 eV in O and 360 eV in N_2. These processes are sensitive to two very narrow EUV wavelength regions.

We found an unexpected noise signal in the photoelectron fluxes that appears to be independent of energy and has some spatial organization. The data suggest that the intensity of the noise signal is ~20% of the intensity of photoelectrons directly produced from solar irradiances. The primary source of the noise is not related to detector sensitivity, is not solely due to an orbital bias in the way the data were accumulated, and appears not to be of anthropogenic origin. It was not possible to determine more about the noise source(s) because the limited data were acquired primarily near the terminator.

Intensifications of the photoelectron flux associated with solar flares is less apparent in the integrated daily flux from 156 eV to 1 keV than it is in daily averages of the flux in individual FAST energy channels. This reflects the fact that most of the contribution to the integral flux comes from the lower energy channels where the flux is higher. Examination of daily averaged photoelectron fluxes at energies between 25 eV and 500 eV show significant changes in the photoelectron spectra in response to X and M class flares.

Comparison of modeled and daily average electron fluxes shows that the HEUVAC model solar spectrum short ward of 25 eV does not reproduce the observed variations of solar intensity over the interval investigated. It follows that higher wavelength resolution than is currently available from the XPS sensor is required to be able to accurately model ionospheric photochemistry.

Finally we note that it might be possible to produce high resolution solar spectra short ward of 45 nm (corresponding to photoelectrons of ~ 12 eV, the lowest reliable energy channel available in the FAST data) by using a forward based model of photoelectron production combined with a statistical least squares fitting technique. Since most of the photoelectron flux in the 100-500 eV region is the result of Auger photoionization processes, this technique will provide information primarily about EUV fluxes at 2.3 and 3 nm. We note also that this technique is best suited to observations made following a large solar flare, as the solar induced changes are much larger then than the noise signals in the photoelectron fluxes documented here.

Acknowledgements

We acknowledge helpful discussions by Dayton Datlowe, Craig Rodger, Jean-André Sauvaud, Frank Eparvier and Robert Meier. This paper was substantially revised in response to constructive comments from the reviewers. Support was provided by NASA Grant NNG05GK153.

References

Abel, B. and Thorne, R.M. Modeling energetic electron precipitation near the South Atlantic anomaly, J. Geophys. Res., 104, 7037-7044, 1999.

Bailey, S.M., Barth, C.A., Erickson, M.J., et al. Science instrumentations for the Student Nitric Oxide Explorer, Proc. SPIE, Int. Soc. Opt. Eng., 2830, 264-273, 1996

Carlson, C.W., McFadden, J.P., Turin, P.D., et al. The electron and ion plasma experiment for FAST, Space Sci. Rev. 98, 33-66, 2001.

Chamberlin, P.C. The flare irradiance spectral model, Thesis, University of Colorado, Department of Aerospace Engineering Sciences, Boulder, Colorado, 2005.

Datlowe, D.W., Imhof, W.L., Fishmanet, G.J., et al. Local time and seasonal variations in the precipitation of energetic electrons from the inner radiation belt by cyclotron resonance with waves from powerful VLF transmitters, Radio Sci., 30, 47-56, 1995.

Doering, J.P., Peterson, W.K., Bostrom, C.O., et al. High Resolution Daytime Photoelectron Energy Spectra from AE-E, Geophys. Res. Lett. 3, 129-132, 1976.

Goembel, L., Doering, J.P., Morrison, D., et al. Atmospheric O/N_2 ratios from photoelectron spectra, J. Geophys. Res. 102, 7411-7420, 1997.

Judge, D.L., McMullin, D. R., Ogawa, H. S., et al. First solar EUV irradiances obtained from SOHO by the CELIASSEM, Sol. Phys. 177, 161–173, 1998.

Hernandez, S.P., Doering, J.P., Abreu, V.J., et al. Comparison of absolute photoelectron fluxes measured on AE-C and AE-E with theoretical fluxes and predicted and measured N_2 2PG 3371Å volume emission rates, Planet. Space Sci., 31, 221-233, 1983.

Lee, J. S., J. P. Doering, T. A. Potemra, and L. H. Brace, Measurements of the ambient photoelectron spectrum from Atmosphere Explorer, I, AE-E measurements below 300 km during solar minimum conditions, *Planet. Space Sci.*, *28,* 947, 1980a.

Lee, J.S., Doering, J.P., Potemra, T.A., et al. Measurements of the ambient photoelectron spectrum from Atmosphere Explorer: II. AE-E measurements from 300 to 1000 km during solar minimum conditions, Planet. Space Sci., 28, 973-996, 1980b.

Peterson, W.K., Doering, J.P., Potemra, T.A., et al. Measurement of magnetic field aligned potential differences using high resolution conjugate photoelectron energy spectra, Geophys. Res. Lett 4, 373-376, 1977.

Richards, P.G., and Torr, D.G., A simple theoretical model for calculating and parameterizing the ionospheric photoelectron flux, *J. Geophys. Res.*, 88, 2155, 1983.

Richards, P.G., and Torr, D.G., An investigation of the consistency of the ionospheric measurements of the photoelectron flux and solar EUV flux, J. Geophys. Res., 89, 5625-5635, 1984.

Richards, P.G., and Torr, D.G., The altitude variation of the ionospheric photoelectron flux: a comparison of theory and measurement," J. Geophys. Res., 90, 2877-2884, 1985.

Richards, P. G., Ion and neutral density variations during ionospheric storms in September 1974: Comparison of measurement and models, J. Geophys. Res., 107, 1361, doi:10.1029/2002JA009278, 2002.

Richards, P.G., Woods, T.N., and Peterson, W.K. HEUVAC: A new high resolution Solar EUV proxy model, Adv. Space Res., 37, 315-322, 2006.
Rodger, C.J., Clilverd, M.A. Inner radiation belt electron, lifetimes due to whistler-induced electron precipitation (WEP) driven losses, Geophys. Res. Lett., 29, 30, 2002 doi: 10.1029/2002GL015795, 2002.
Rodger, C.J., Cliverd, M.A. and Dowden, R.L. D region reflection height modification by whistler-induced electron precipitation, J. Geophys. Res., 107, 1145, doi: 10.1029/2001JA000311, 2002.
Santolík, O., Němec, F., Parrot, M., et al. Analysis methods for multi-component wave measurements on board the DEMETER spacecraft, Planetary and Space Science, 54, 512-527, 2006.
Sauvaud, J.A., Moreau, T., Maggiolo, R., et al. High-energy electron detection onboard DEMETER: The IDP spectrometer, description and first results on the inner belt, Planetary and Space Science, 54, 502-511, 2006
Solomon, S.C. and Quan, L. Solar extreme-ultraviolet irradiance for general circulation models, J. Geophys. Res., 110, A10306 , doi:10.1029/2005JA011160, 2005
Strickland, D.J., Lean, J.L., Meier, R.R., et al. Solar EUV irradiance variability derived from terrestrial far ultraviolet dayglow observations, Geophys. Res. Lett., 31, L03801, doi:10.1029/2003GL018415, 2004.
Su, Y., Horwitz, J. L., Wilson, G. R., et al. Self-consistent simulation of the photoelectron-driven polar wind from 120 km to 9 R_E altitude, J. Geophys. Res., 103, 2279-2296, 1998.
Warren, H.P., Mariska, J.T., and Lean, J. A new model of Solar EUV irradiance variability: 1, Model formulation, J. Geophys. Res., 106, 15745-15758, 2001.
Winningham, J. D.,. Decker, D. T., Kozyra J. U., Nagy A. F., and J. R. Jasperse, Energetic (>60 eV) atmospheric photoelectrons, J. Geophys. Res., 94(A11), 15,335–15,348, 1989.
Woods, T.N. Eparvier, F., Bailey, S., et al. TIMED Solar EUV experiment, SPIE, 3442, 180-191, 1998.
Woods, T.N. and Rottman, G.J. Solar ultraviolet variability over time periods of aeronomic interest, in Comparative Aeronomy in the Solar System, Mendillo, M., Nagy, A., and Waite, Jr., J. Hunter. (eds). Geophys. Monograph Series, Wash, DC, 221-233, 2002.
Woods T.N., Bailey, S.M., Peterson, W.K., et al. Solar extreme ultraviolet variability of the X-Class flare on April 21, 2002 and the terrestrial photoelectron response, Space Weather, 1, 1001, doi:10.1029/2003SW000010, 2003.
Woods, T.N., F.G. Eparvier, S.M. Bailey, P.C. Chamberlin, J. lean, G.J. Rottman, S.C. Solomon, W.K. Tobiska, D.L. Woodraska, The Solar EUV Experiment (SEE): Overview and prime mission results, J. Geophys. Res., 110, A01312, doi:10.1029/2004JA010765, 2005.

Figures

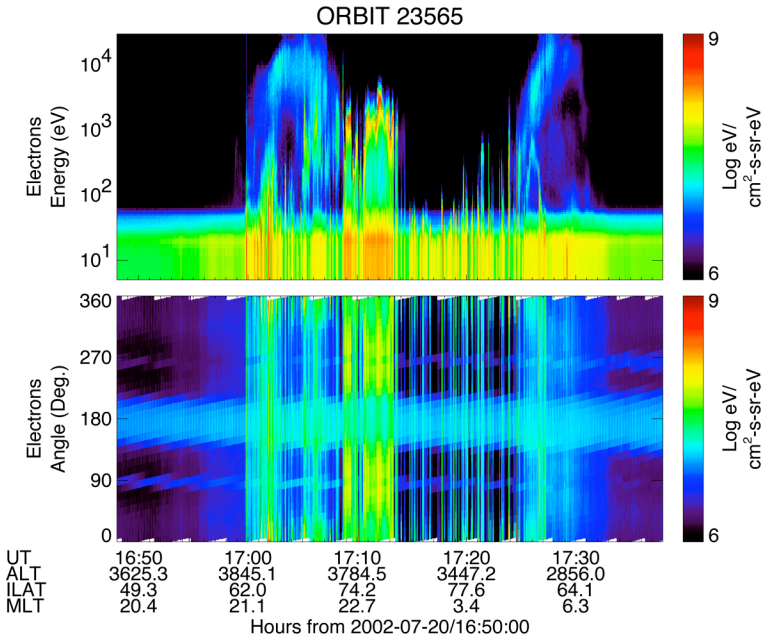

Figure 1: Energy time and angle time spectrogram of data acquired from FAST on July 20, 2002. The top panel presents the upflowing energy flux within 30^o of the magnetic field line. The intensity in units of (eV/cm^2-s-sr-eV) has been encoded using the color bar on the right. The second panel presents the angular distribution of the energy flux from 6 eV to 30 keV. Electron pitch angle in the range 0-180^o is related to the angle shown as follows: From 0-180^o pitch angle equals the angle shown; from 180-360^o pitch angle equals 360^o minus the angle shown. The intensity in units of (eV/cm^2-s-sr-eV) has been encoded using the color bar on the right. The FAST altitude (ALT) in kilometers, invariant latitude (ILAT) in degrees, magnetic local time (MLT) in decimal hours of day, and universal time (UT) the data were acquired are shown at the bottom.

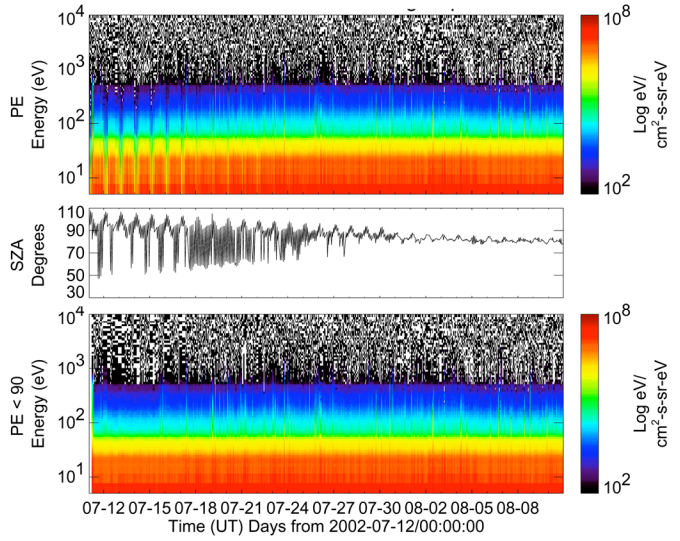

Figure 2: Summary of upward flowing electrons observed from July 10 to August 10, 2002. Top panel: energy-time spectrum of all one-minute average spectra acquired equatorward of the auroral oval available for analysis. The number flux in units of $(cm^2\text{-}s\text{-}sr\text{-}eV)^{-1}$ is encoded by the color bar on the right. Second panel: Solar Zenith Angle (SZA) in the ionosphere at the foot points of magnetic field lines passing through the FAST satellite. Bottom panel: The sub-set of data for which the SZA is less than 90^o.

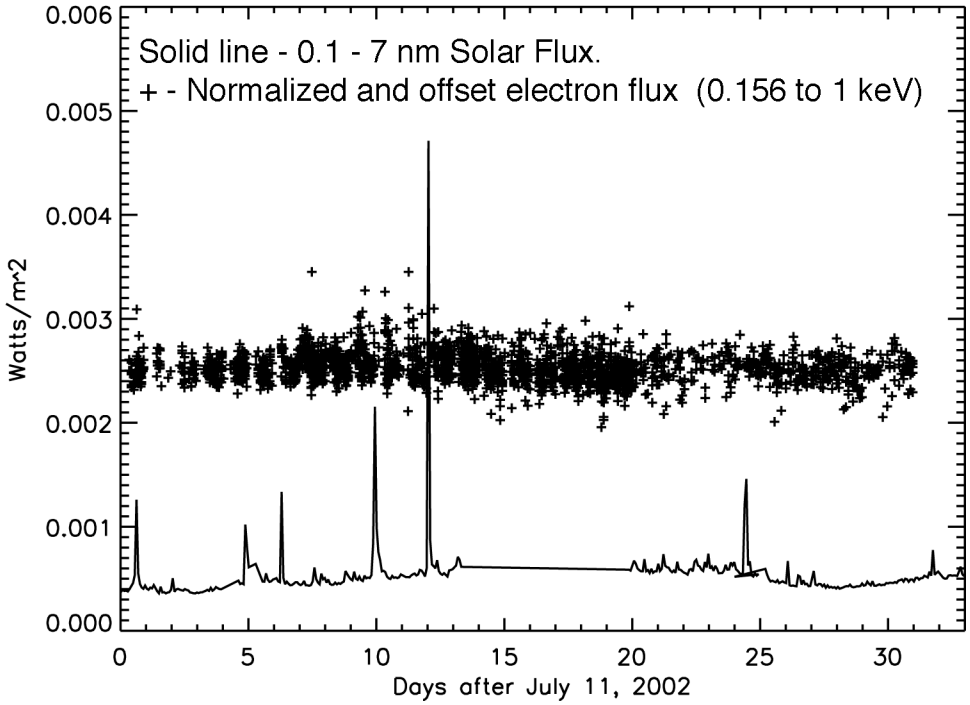

Figure 3. Observed solar irradiance in the 0.1 to 7 nm bin and that inferred from 0.156 to 1 keV photoelectron data. The photoelectron data have been normalized to the solar power. The photoelectron data have been offset by 0.002 W/m^2 to aid visualization.

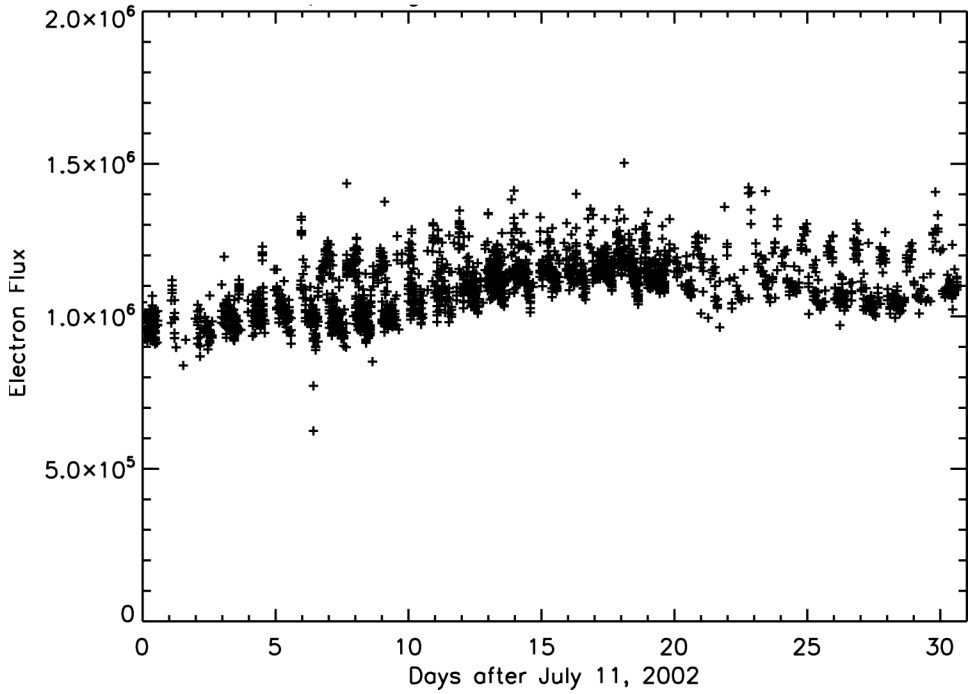

Figure 4. Observed upflowing electrons from the FAST energy channel centered on 41 eV obtained from the 2416 one-minute average spectra presented in the bottom panel of Figure 2.

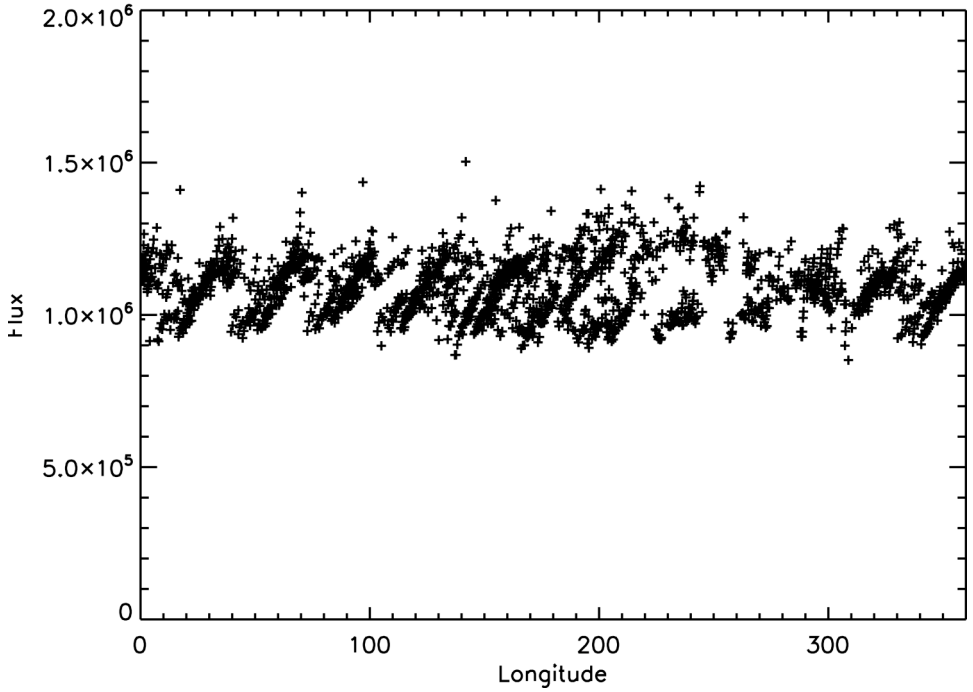

Figure 5. Observed upflowing 41 eV electrons shown in Figure 4 organized by the longitude of the closest ionospheric foot point passing through the FAST satellite.

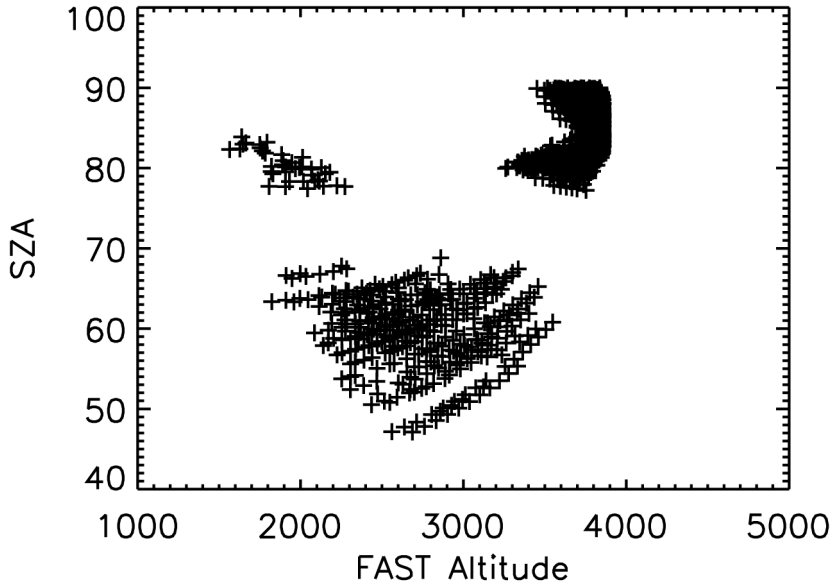

Figure 6. Location of the FAST Satellite in km of altitude and degrees of solar zenith angle for the 2416 photoelectron spectra used in this investigation.

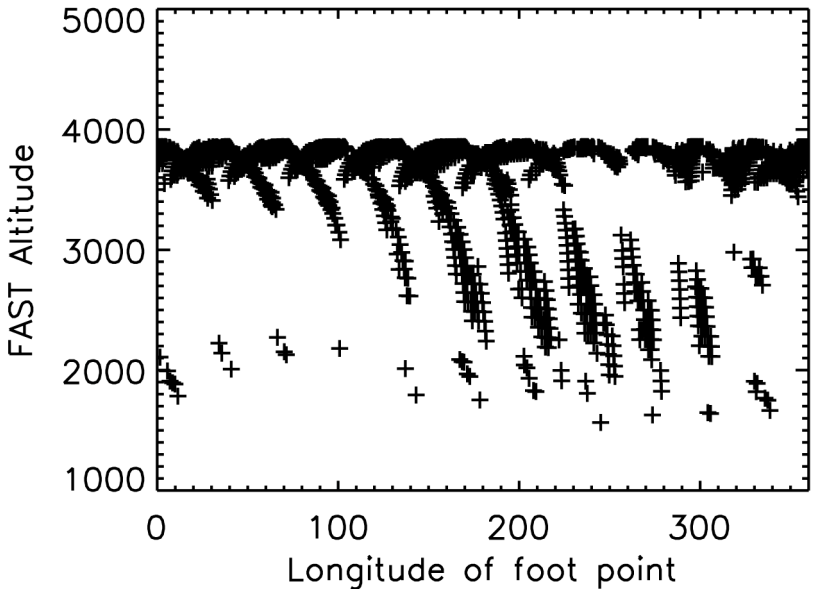

Figure 7. Location of the foot point of a magnetic field line through the FAST satellite as vs. the FAST altitude at the time each of the 2416 photoelectron spectra used in this investigation were acquired.

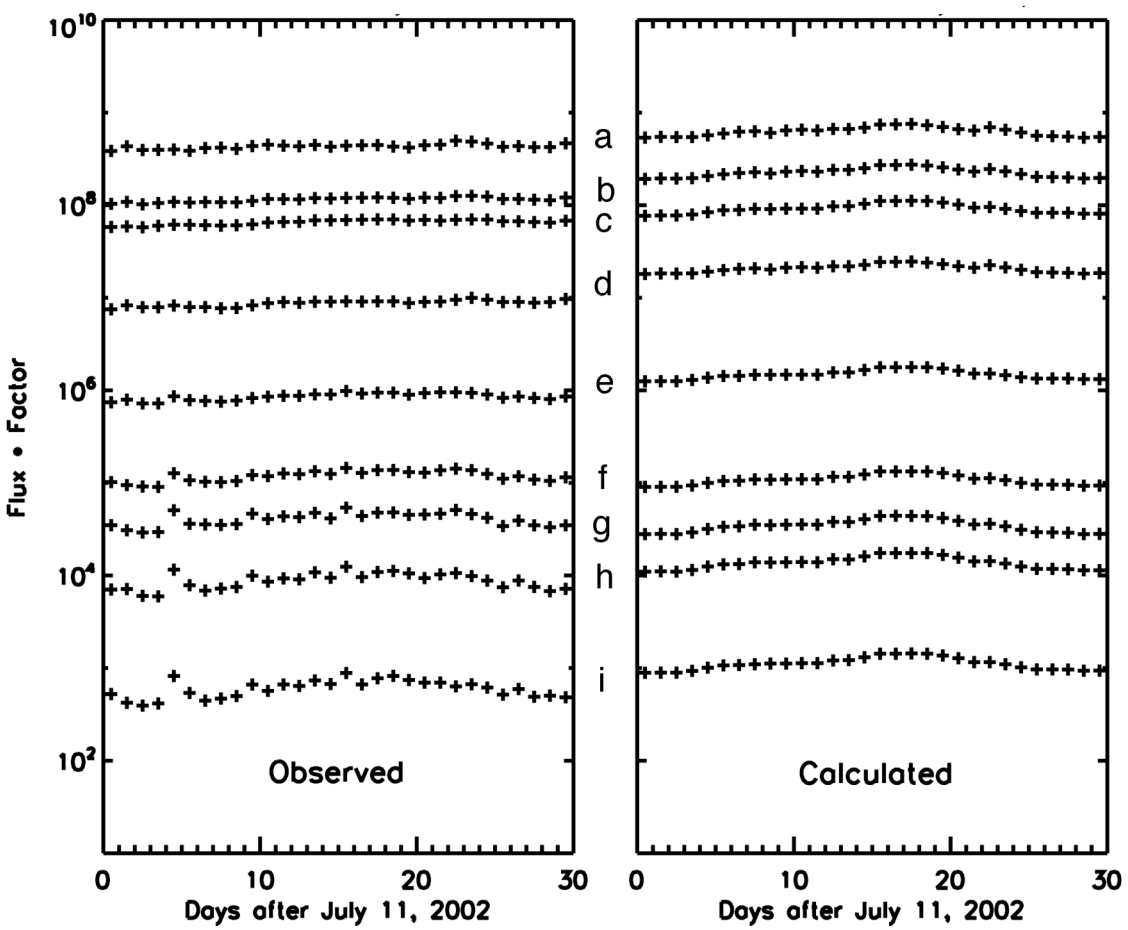

Figure 8. Observed (left) and calculated (right) daily average photoelectron fluxes from July 11 to August 10 2002 from selected energy channels. The flux units are $(cm^2\text{-s-sr-eV})^{-1}$ times a factor dependent on the energy displayed. The energies and factors are: a (25 eV / 80), b (33 eV / 70), c (41 eV / 60), d (57 eV / 50), e (98 eV / 40), f (196 eV / 30), g (298 eV / 20), h (392 eV / 10), and i (486 eV / 1).